PERGAMON

Journal of Atmospheric and Solar-Terrestrial Physics 62 (2000) 1115–1127

Journal of ATMOSPHERIC AND SOLAR-TERRESTRIAL PHYSICS

www.elsevier.nl/locate/jastp

Upper-atmospheric effects of magnetic storms: a brief tutorial

A.D. Richmond*, G. Lu

High Altitude Observatory, National Center for Atmospheric Research (NCAR), P.O. Box 3000, Boulder, CO 80307-3000, USA

Received 1 December 1999; accepted 3 April 2000

Abstract

The physical processes underlying several phenomena of upper-atmospheric storms are described: magnetospherically driven ion convection and Joule heating and their impact on the high-latitude thermosphere and ionosphere; global changes in thermospheric circulation and composition; traveling atmospheric disturbances; and effects of electric-field penetration to middle and low latitudes. Examples from the 1997 January 10–11 storm are used to illustrate some of these features. It is pointed out that not only the magnitude, but also the sign of many storm-time changes at any given location depend sensitively on the temporal and spatial variations of auroral particle precipitation and high-latitude electric fields. In order for simulation models to be able to predict upper-atmospheric storm effects accurately, improved determination of the high-latitude inputs will be required.

Keywords: Upper-atmospheric effects; Magnetic storms; Magnetospheric disturbances

1. Introduction

Upper-atmospheric storms occur as a result of greatly increased auroral particle precipitation and high-latitude ionospheric electric fields and currents lasting several hours or more during magnetospheric disturbances. The ensuing high-latitude ionization, Joule heating, and ion-drag forcing of the upper atmosphere, along with penetration of the electric fields to low latitudes, affect the global dynamics and structure of the thermosphere and ionosphere. The thermosphere heats and expands; its composition is altered; traveling gravity-wave disturbances emanate from the polar regions; and the ionospheric plasma density increases, decreases, or is redistributed by winds and electric fields. Many reviews of upper-atmospheric storm effects have appeared in recent years (Rishbeth, 1991; Prölss, 1995,1997; Rees, 1995; Schunk and Sojka, 1996; Fuller-Rowell et al., 1997; Abdu, 1997; Buonsanto, 1999), which can be consulted for comprehensive discussions of previous work in this field. The aim of the present paper is to describe some of the basic upper atmospheric properties that help determine the nature of storm effects, and to summarize some selected storm effects on the upper atmosphere, with a view toward identifying a major research need for developing a forecasting capability of these effects. The case of the 1997 January 10–11 storm is used as a particular emphasis. This storm has already received considerable attention (Lu et al., 1998; Steele and McEwen, 1998; Spann et al., 1998; Elsen et al., 1998; Ho et al., 1998; Sánchez et al., 1998; Rees et al., 1998; Hairston et al., 1999; Sivjee, 1999; Schlegel and Collis, 1999; McEwen et al., 1999; Mikhailov and Förster, 1999; Jakowski et al., 1999; Aarons and Lin, 1999; Buonsanto et al., 1999).

Fig. 1 shows typical densities of different constituents of the upper atmosphere. The portion of the atmosphere above about 90 km, where temperature increases with height up to values of 500–2000 K at high altitudes, is called the thermosphere. Within it is embedded the ionosphere, which comprises only a small fraction of the total upper-atmospheric density. The ionospheric plasma is created as the neutral constituents are ionized by sunlight and by precipitating energetic auroral particles, and

* Corresponding author. Tel.: +1-303-497-1570; fax: +1-303-497-1589.

E-mail address: richmond@ucar.edu (A.D. Richmond).

1364-6826/00/$ - see front matter
PII: S1364-6826(00)00094-8

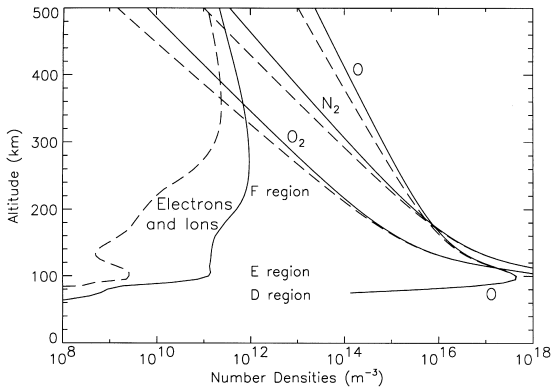

Fig. 1. Typical number densities of neutral and ionized species for noon (solid) and midnight (dashed) at 44.6°N, 2.2°E on March 21 for medium solar activity (10.7 cm radio flux of 120×10^{-22} W cm^{-2} Hz^{-1}; sunspot number 67) and low magnetic activity ($A_p = 4$), obtained from the 1990 International Reference Ionosphere (Bilitza, 1990) and the MSISE-90 neutral-density model (Hedin, 1991). The ionospheric regions conventionally called D, E, and F are also indicated.

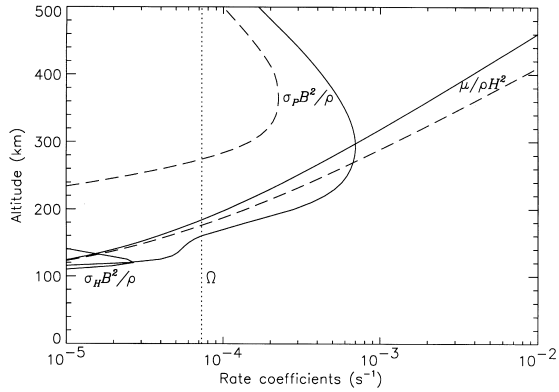

Fig. 2. Typical rate coefficients for noon (solid) and midnight (dashed) for the same conditions as in Fig. 1. The rate for diffusive effects is represented by the coefficient of molecular viscosity, μ, divided by mass density ρ and by the square of the pressure scale height H. The Pedersen and Hall ion drag coefficients are $\sigma_P B^2/\rho$ and $\sigma_H B^2/\rho$, where σ_P, σ_H are the Pedersen and Hall conductivities and B is the geomagnetic-field strength. The vertical dotted line is the angular rotation rate of the Earth Ω, representative of the time-rate-of-change for diurnal changes in the upper atmosphere and of Coriolis effects.

it is destroyed by chemical reactions that eventually lead to recombination of the ions and free electrons. The atmosphere is gravitationally stratified, and its density decreases exponentially with increasing height. The exponential scale height depends on the temperature and mean molecular mass, and varies from about 5 km at the base of the thermosphere to roughly 50 km to 500 km height. The density at high altitudes depends very sensitively on changes in the scale height, which varies with solar cycle, time of day, and magnetic activity. The density can vary by two orders of magnitude above 400 km, obviously a factor of concern when trying to predict the effects of atmospheric drag on low-Earth-orbiting satellites.

The mean free path of molecules increases with height as the density decreases, and diffusion of mass, momentum, and heat proceed increasingly rapidly with altitude. Turbulent mixing ceases above about 110 km, and the different atmospheric constituents are free to separate gravitationally according to their individual molecular weights. O_2 molecules are broken apart by photochemical processes, producing O atoms, which become the dominant constituent at upper thermospheric altitudes. The density ratios $[O]/[N_2]$ and $[O]/[O_2]$ increase monotonically with height, a fact that is important when considering how thermospheric composition is affected by vertical motions. Even though the heavy molecular species N_2 and O_2 normally have small densities in the upper thermosphere, they determine the loss rate of ionospheric ions, and variations in their densities are very important for the F-region ionosphere. Above about 200 km the loss rate of the dominant ion O^+ is determined by the reactions

$$O^+ + N_2 \rightarrow NO^+ + N,$$

$$O^+ + O_2 \rightarrow O_2^+ + O$$

whose ionic products NO^+ and O_2^+ are destroyed almost immediately by recombination with electrons. Therefore, if the N_2 and O_2 densities increase during a storm, ionospheric plasma is depleted.

Molecular diffusion affects mass, momentum, and heat all on similar time scales. One can define at each height a characteristic diffusive rate (D/H^2, where D is the diffusion coefficient and H the pressure scale height) that represents the rate at which diffusive effects tend to bring all higher levels into diffusive equilibrium, having vertically uniform winds and temperatures. Fig. 2 shows the closely related viscous rate, $\mu/\rho H^2$, where μ is the coefficient of viscosity, and ρ is mass density, for typical thermospheric conditions. Characteristic diffusive time scales (the inverses of the rates) are about 1 day at 125 km, and 1 h at 240 km. Perturbations in the composition, temperature, and wind at one altitude are rapidly transmitted by diffusion to higher altitudes, but more slowly to lower altitudes. The more massive lower levels act as a sink of heat and momentum for the higher levels, so that the structure of the higher levels of the thermosphere always depends on the structure of the lower levels. When the thermosphere is disturbed, the time it takes to relax back to its initial state depends in part on the longest diffusive time scale in the disturbed region, which is found at the lowest disturbed altitude. (For temperature disturbances, radiative cooling also comes into play with a time scale on the order

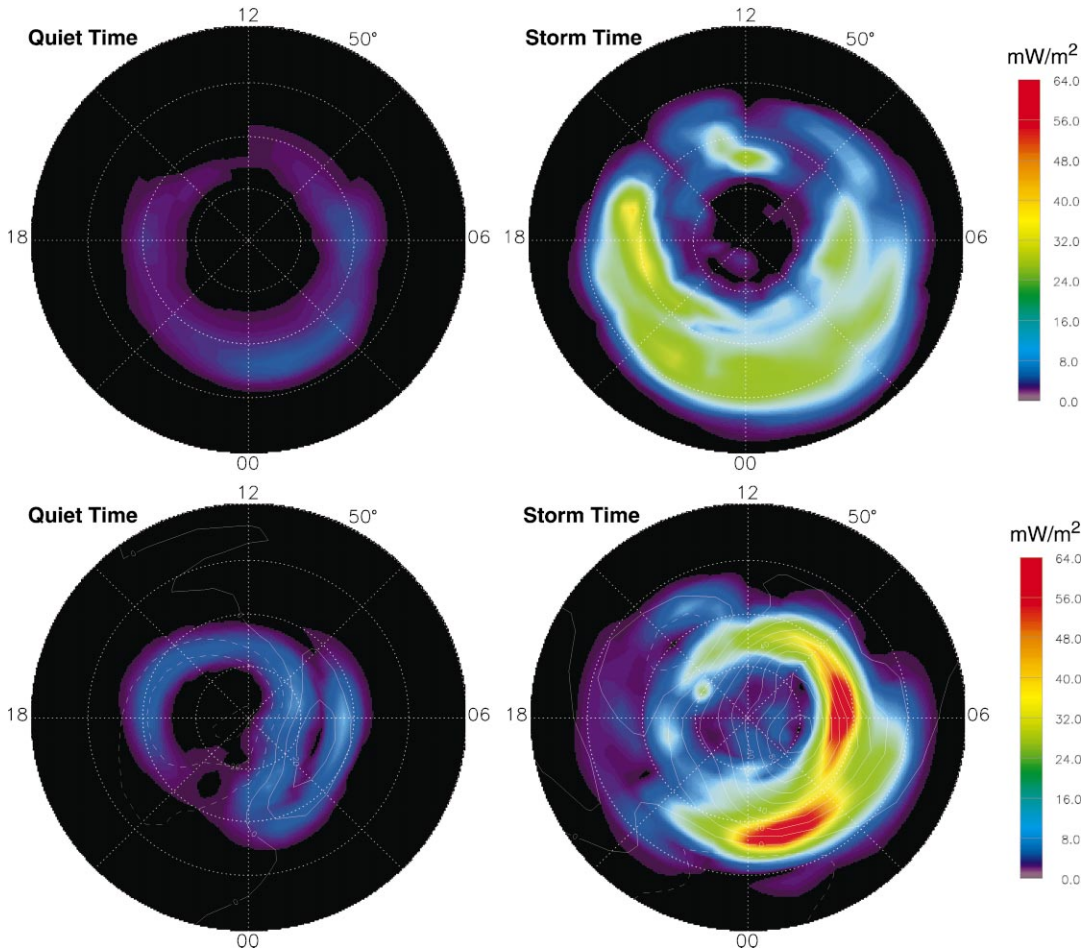

Fig. 3. Distributions in magnetic latitude and magnetic local time of the estimated auroral electron energy flux (top), the height-integrated Joule heating rate (bottom, colors), and the electric potential (bottom, overlain contours) above 50° magnetic latitude in the northern hemisphere for two times on 1997 January 10: 0255 UT (left), a quiet period, and 1105 UT (right), an active time. The electric-potential contour interval is 10 kV.

of a day, as demonstrated by Maeda et al. (1989), Burns et al. (1989), and Field et al. (1998).) During magnetic storms, for example, the thermosphere can be significantly heated at all altitudes above about 120 km, although the temperature change is generally largest at high altitudes. During recovery from the storm, the high altitudes relax relatively quickly, but it may require up to days for all altitudes down to 120 km to recover completely back to their undisturbed state. Similar statements can be made regarding the time for disturbed winds and composition to relax back to the quiet state.

To illustrate storm effects we focus on the event of 1997 January 10–11. Lu et al. (1998) have analyzed the energetics of this storm by assimilating a large amount of ground- and space-based observations with the assimilative mapping of ionospheric electrodynamics (AMIE) procedure. Fig. 3 shows examples of the distributions of the auroral electron energy flux and of the electric potential and height-integrated Joule heating over the northern polar region, for a quiet time (0255 UT, left) and a disturbed time (1105 UT, right) on 1997 January 10. Most of the auroral electron energy tends to be deposited in the 90–150 km altitude region, while the Joule heating is generated mostly in the 115–150 km height region, although some extends to higher altitudes as well. Fig. 4 shows the time history of various global parameters: the interplanetary magnetic field (IMF) strength and the IMF northward component (B_z); the auroral electrojet (AE) indices; the total electric potential drops in the northern and southern hemispheres; and the rates of hemispherically integrated Joule heating and energy deposition by auroral electron precipitation in each hemisphere. The energy inputs to the upper atmosphere began increasing on January 10 around 4 UT, and continued in the northern hemisphere until around 20 UT. In the southern hemisphere significant Joule heating continued after the IMF B_z turned northward.

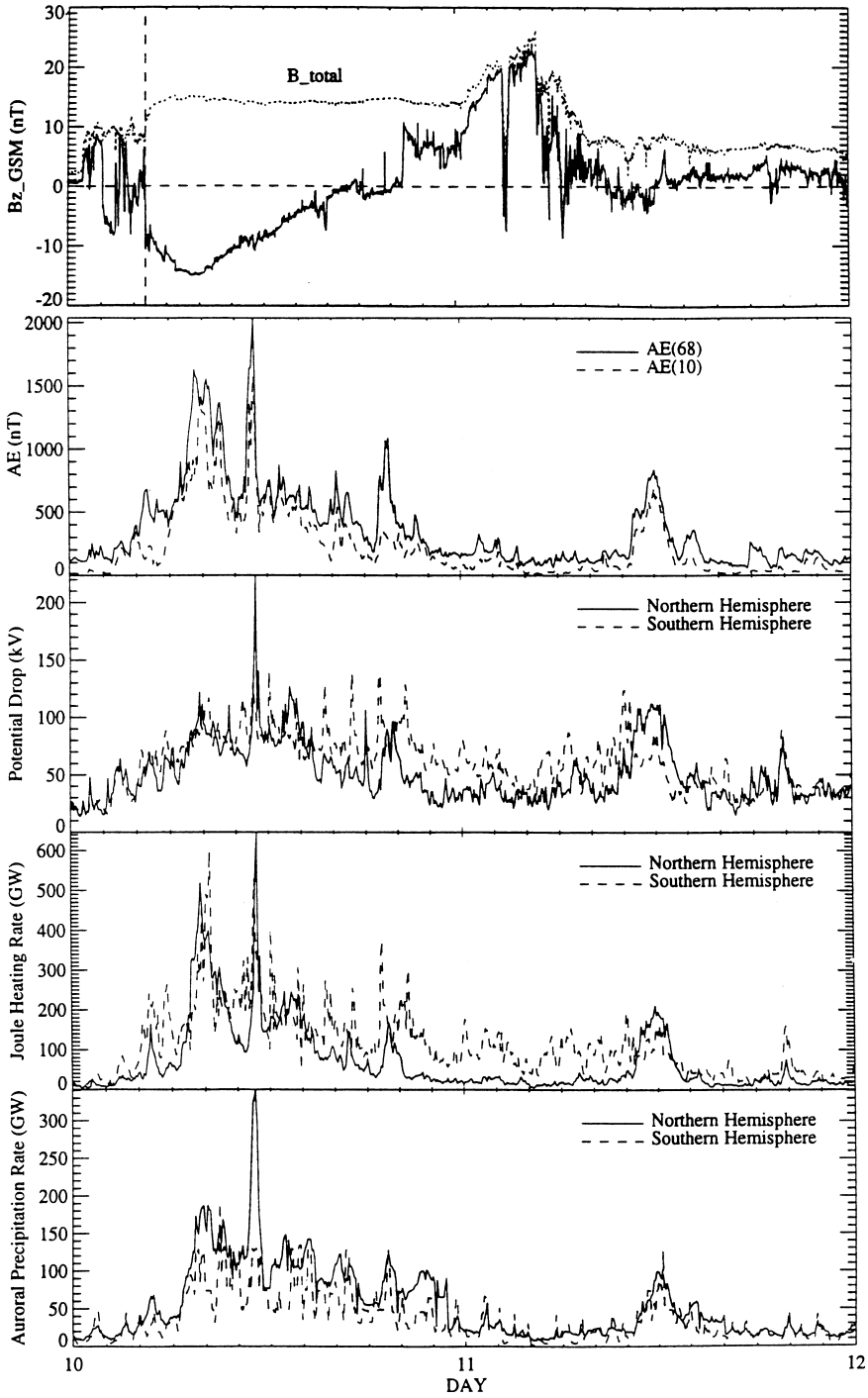

Fig. 4. Interplanetary and geophysical quantities for the two-day period 1997 January 10–11. On top are the interplanetary magnetic field strength (B_total) and the northward component in geocentric solar ecliptic (GSM) coordinates (Bz_GSM). Next are the auroral electrojet (*AE*) indices derived from all available (68) northern-hemisphere magnetometers [*AE*(68)], and from 10 selected magnetometers that are part of the standard network for computing the *AE* indices [*AE*(10)]. Next are the total electric potential drops (the differences between the maximum and minimum potentials) in the northern and southern hemispheres. The bottom two frames show the rates of hemispherically integrated Joule heating and energy deposition by auroral electrons in each hemisphere. (From Lu et al., 1998. Copyright by the American Geophysical Union.)

The pulses of Joule heating like those around 8 UT and 11 UT produced traveling atmospheric disturbances.

2. Effects in the polar ionosphere/thermosphere

The high-latitude region is where most of the energy is transferred from the magnetosphere to the thermosphere during magnetic storms. The spatial distributions of the auroral energy deposition and of Joule heating can be quite different at any given time, as seen at 1105 UT in Fig. 3. The total hemispheric Joule heating is usually larger than the energy deposited by auroral electrons during a storm, as seen in Fig. 4. Joule heating is considerably more effective than the energy of the auroral electrons in affecting the thermospheric circulation, not only because of greater energy input, but also because much of the auroral particle energy is deposited at lower altitudes where the denser gas is more difficult to perturb, and because only about 1/2 of the auroral particle energy goes directly into heat (Rees et al., 1983). However, the auroral energy is very important for the composition and energetics of the lower thermosphere due to its ionizing role and its influence on creating minor species like nitric oxide that are chemically and radiatively active.

The auroral precipitation enhances the ionospheric electrical conductivity, and facilitates horizontal current flow across geomagnetic field lines through the ionosphere. Much of this current flow is connected to field-aligned currents above the ionosphere. During disturbed periods the strong electric fields produce rapid plasma convection, largely horizontal but also with an important vertical component where the magnetic field is tilted a little from the vertical. Since the ionosphere is strongly horizontally stratified, vertical drifts have a much larger influence on the plasma distribution than do horizontal drifts, but the latter can also be important.

The structure of the polar ionosphere can be very complex. The horizontal convection is rapid enough to move significant amounts of plasma from the dayside into and across the polar cap, producing tongues and patches of enhanced ionospheric density in the dark polar cap (e.g. Schunk and Sojka, 1996; Sojka et al., 1998). Deep depletions of plasma density can be produced by several mechanisms (Schunk et al., 1976): nighttime decay in regions of stagnant total plasma flow (convection plus corotation); enhanced ion loss rates due to elevated ion temperatures and vibrationally excited N_2 molecules caused by frictional heating in regions of rapid ion convection; increased polar-wind flow of plasma out the top of the ionosphere; and increased loss due to augmented neutral molecular densities in regions of upward vertical winds. Auroral particle precipitation creates highly structured enhancements of plasma density. Strong gradients in the flow velocities and in the plasma densities give rise to plasma instabilities and irregularities (e.g. Aarons and Lin, 1999). These irregularities enable radars like the SuperDARN system (Greenwald et al., 1995) to obtain backscattered echoes and measure the convection, but they also degrade radio-wave transmissions from spacecraft.

The neutral thermosphere is also affected by the electric fields and currents, and the storm-time changes in the neutrals further influence the ionosphere. The current has two effects on the thermosphere. First of all, when the convecting ions collide with the neutrals, they transfer momentum to the thermospheric gas, and tend to accelerate the gas in the direction of the ion motion. This is often called "ion-drag" acceleration (or deceleration, if the ion velocity is less than, or oppositely directed to, the neutral velocity). Macroscopically, it is the Ampère acceleration produced on the medium by an electric current flowing through a magnetic field, sometimes also referred to as the Lorentz acceleration. We denote it $\mathbf{a}_A$. It is proportional to the ion density, and to the difference between the ion and neutral bulk velocities. It can also be expressed in terms of the component of the neutral bulk velocity perpendicular to the geomagnetic field, $\mathbf{u}_\perp$, and the electromagnetic convection velocity, $\mathbf{v}_E \equiv \mathbf{E} \times \mathbf{B}/B^2$, where $\mathbf{E}$ is the electric field and $\mathbf{B}$ is the geomagnetic field, as

$$\mathbf{a}_A = \frac{\sigma_P B^2}{\rho}(\mathbf{v}_E - \mathbf{u}_\perp) + \frac{\sigma_H B}{\rho}\mathbf{B} \times (\mathbf{v}_E - \mathbf{u}_\perp), \quad (1)$$

where σ_P and σ_H are the Pedersen and Hall conductivities and ρ is total mass density. The midlatitude values of the ion-drag coefficients $\sigma_P B^2/\rho$ and $\sigma_H B^2/\rho$ shown in Fig. 2 give an idea of the relative importance of ion drag to viscous effects. In the auroral zone, the values of the coefficients below 200 km can be strongly enhanced by particle precipitation, and often exceed the midlatitude daytime values of Fig. 2 even at night. The electrodynamic velocity $\mathbf{v}_E$ is usually considerably larger than the wind velocity $\mathbf{u}$ at high latitudes during storms, and so $\mathbf{a}_A$ can become a primary force on the neutral gas even when the ion-drag coefficients have modest values.

Fig. 5 shows a snapshot of the ion convection velocity (right) and of the neutral wind velocity (left) at 134 km altitude on 1997 January 10 at 8 UT, from a simulation of this storm using the NCAR Thermosphere-Ionosphere-Electrodynamics General Circulation Model (TIE-GCM). Notice that the vector scales differ by about a factor of 3. The imprint of the ion convection on the neutral motion is clear, but the patterns and strengths differ because inertia causes a significant time delay of the neutrals to the ion-drag acceleration. The acceleration of the neutral gas occurs primarily above 115 km, because below that height ion-neutral collisions become so frequent that the ions are significantly slowed down, and no longer convect at the electrodynamic velocity $\mathbf{v}_E$. The greatest direct acceleration of the thermosphere occurs in the F region, where the electron density is largest, but the viscous coupling between the different heights tends to smooth out vertical gradients of the winds there. Because of the exponential decrease of mass density with height, viscous coupling tends to impose the wind

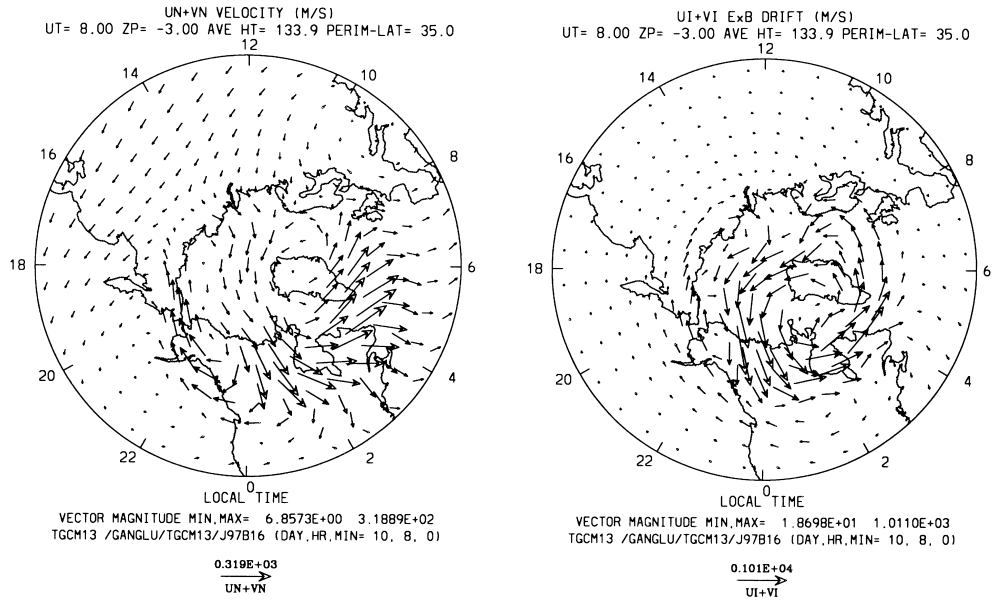

Fig. 5. Distributions in geographic latitude and solar local time of the horizontal wind velocity **u** (left) and the electromagnetic convection velocity $\mathbf{v}_E$ (right) at about 134 km altitude for latitudes above 35° in the northern hemisphere on 1997 January 10 at 0800 UT, simulated by the NCAR TIE-GCM. Notice the difference in velocity scales: the longest vector is 319 m/s for **u** but 1010 m/s for $\mathbf{v}_E$.

velocities from the lower levels onto higher levels of the thermosphere, with coupling time constants determined by the viscous time scales like those illustrated in Fig. 2.

The second important way that electric currents and fields affect the thermosphere is through Joule heating. This can be viewed as the frictional heating produced in the gas as the rapidly convecting ions collide with neutral molecules. Like the Ampère acceleration, the heating per unit mass is proportional to the ion density, but the heating is more strongly dependent than the acceleration on the ion-neutral velocity difference, being proportional to the square of that difference. Joule heating is therefore very sensitive to the strength of the electric field, as apparent in Fig. 3. Although most of the Joule heat is deposited at altitudes where the Pedersen conductivity is largest, around 125 km, the atmospheric response depends to some extent on the heating per unit mass, which varies in altitude approximately like the Pedersen conductivity divided by the neutral mass density, and varies in height in a manner similar to the Pedersen ion-drag coefficient $\sigma_P B^2/\rho$.

3. Global circulation and composition

The Joule heating affects the thermosphere in a number of ways. Locally, it heats the gas and causes expansion of the thermosphere. The locally heated gas will be more buoyant than its surroundings, causing it to rise. Vertical velocities of 100 m/s or more can be produced (Smith, 1998). During a storm, auroral heating will alter the mean global circulation of the thermosphere. Fig. 6 shows a model simulation by Brinkman et al. (1992) of the longitudinally averaged meridional circulation of the thermosphere during a storm. Whereas for quiet conditions there is a general upwelling in the summer hemisphere, flow toward the winter hemisphere at higher levels, and downwelling in the winter hemisphere, storm-time heating adds a polar upwelling and equatorward flow in both hemispheres. It can be strong enough to reverse the poleward flow in the winter hemisphere. In addition to affecting the vertical and meridional wind velocities, this circulation has other important effects. The increased downwelling (or reduced upwelling) at midlatitudes moves the air into regions of increasing pressure, and produces compressional heating. Thus the auroral heating is spread worldwide. Storm-time temperatures can increase by several hundred kelvins, and the expansion of the thermosphere causes large atmospheric density increases at high altitudes.

The equatorward wind is acted upon by the Coriolis force, and turns westward. That is, the equatorward wind carries angular momentum from high to lower latitudes: the expansion of the radius of the ring of air is accompanied by a reduction in its angular velocity. Rotating less rapidly than the Earth, it appears to move westward as viewed from the Earth. The westward wind can continue to build up and become considerably larger than the equatorward wind at midlatitudes.

The increased equatorward (or decreased poleward) wind at middle latitudes tends to push the ionosphere higher up

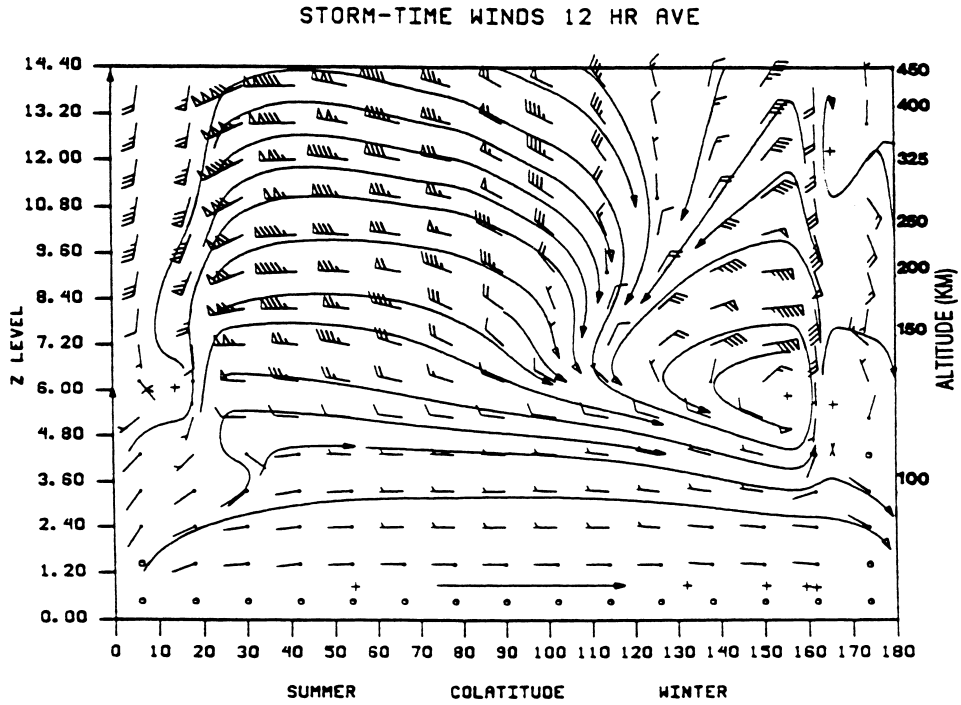

Fig. 6. Twelve-hour-averaged meridional winds and streamlines from a two-dimensional simulation of storm-time thermospheric circulation during northern summer. The horizontal coordinate is colatitude, from 0° at the north pole to 180° at the south pole. The vertical scale is linear in the negative logarithm of pressure (Z level, defined to be zero at 80 km). A nonlinear geometric altitude scale is shown on the right. The wind arrows are rotated to align with the streamlines, which distort the apparent amplitude of vertical motions because of the different vertical and horizontal scales. The barb notation on the wind arrows represents the magnitude of the horizontal meridional wind as follows: short barb (5 ms^{-1}); long barb (10 ms^{-1}); and flag (50 ms^{-1}). (From Brinkman et al., 1992. Copyright by the American Meteorological Society.)

along magnetic field lines, where the loss rate is lower. This can contribute to a positive ionospheric storm effect, i.e., an increase in the electron density. The circulation also causes mixing of the thermospheric gases. At high latitudes the upwelling brings air rich in the heavy molecular constituents N_2 and O_2 to high altitudes, and if the storm heating is sufficiently intense and long-lasting, the circulation carries this molecular-rich air to midlatitudes, especially in the summer hemisphere, where the mean meridional circulation is already equatorward (e.g. Fuller-Rowell et al., 1996; Field et al., 1998). At lower latitudes, the downwelling tends to have the opposite effect: air with low concentrations of molecular species is carried downward, reducing their concentrations at all altitudes. Thus at the higher latitudes the molecular species are enhanced, and at lower latitudes they are depleted. Since these species determine the loss rate of ions, the loss rate is increased at higher latitudes and decreased at lower latitudes, contributing to decreases or increases of electron density.

In reality the effects are not longitudinally symmetric, but have substantial day-night differences in terms of equatorward wind and the transition latitude from enhanced to depleted molecular species. These differences are reflected in the variations of ionospheric storm response at different local times (Wrenn et al., 1987; Rodger et al., 1989; Fuller-Rowell et al., 1994). Prölss (1981, 1993) analyzed satellite observations of the composition and developed a model in which the outflow from the auroral region is strongest at night, and the rotation of the Earth carries the molecular-enriched air into the morning sector, where the molecular enhancement is strongest. During the day the storm outflow is usually counteracted by the normal daytime poleward flow, except for major storms, so that existing composition disturbances usually tend to retreat poleward (Fuller-Rowell et al., 1994), and decay through diffusion. In the afternoon and evening the midlatitude composition disturbance therefore tends to be small. The boundary between molecular enrichment and depletion varies with season, being sharper and lying at higher latitude in winter as compared with summer (e.g. Prölss and von Zahn, 1977). Its location varies not only with local time but also with altitude and with the strength and duration of the Joule heating.

Fig. 7 shows the consequences of this composition effect on the height-integrated electron density, or total electron

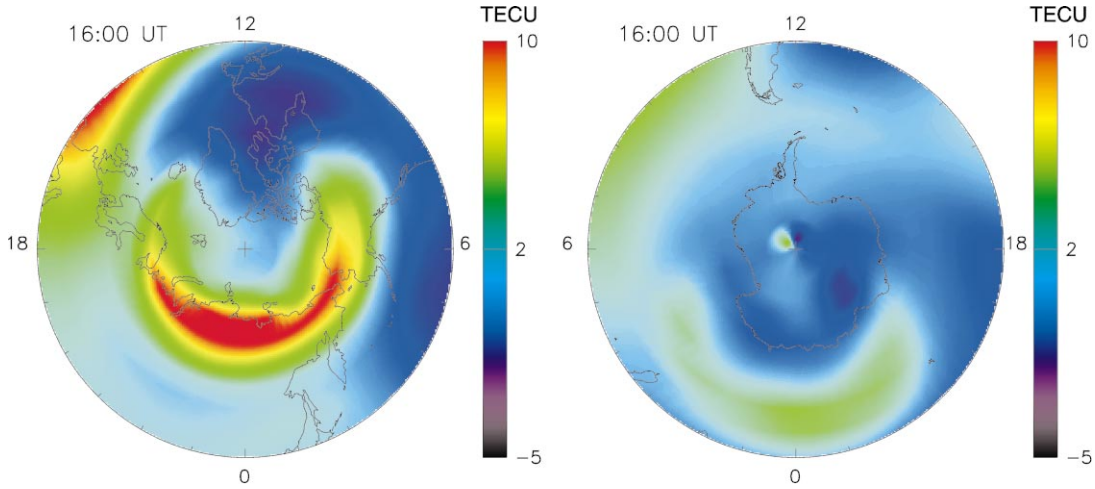

Fig. 7. Distributions above 42.5° geographic latitude in the northern (left) and southern (right) hemispheres of changes in Total Electron Content (TEC) on the storm day 1997 January 10 with respect to a reference quiet day, simulated with the NCAR TIE-GCM. Local noon is at the top. One TECU represents 10^{16} electrons per square meter.

content (TEC), from a simulation of the 1997 January 10 storm with the NCAR TIE-GCM. This figure shows differences in TEC from a reference quiet day at 16 UT, about 10 h after the initial enhancement of the storm-time Joule heating. In the northern hemisphere, there is a storm-time increase of TEC in the auroral oval due to auroral ionization, but there is also an increase at lower latitudes in the afternoon due to more-equatorward winds and to an increase in the density ratio of O to molecular species. There is a depletion of TEC in the morning sector at midlatitudes (the dark blue region), due to a decrease in the ratio of O to molecular species. The southern hemisphere in this simulation does not show such a clear delineation between the enhancements and depletions.

Fig. 8 shows five days of peak ionospheric electron density (NmF2) variations at Millstone Hill (55°N magnetic latitude), while Fig. 9 shows for the last two of these days (January 9 and 10) the peak density, the height of the peak, the vertical ion velocity, and the meridional neutral wind at the Arecibo IS radar (30°N magnetic latitude) and at the nearby Ramey ionosonde (Buonsanto et al., 1999). On January 10, there was a large depletion in NmF2 at Millstone Hill but a large increase at Ramey. The TIE-GCM finds storm-time changes generally in the same sense as observed, although not as big a depletion as observed at Millstone.

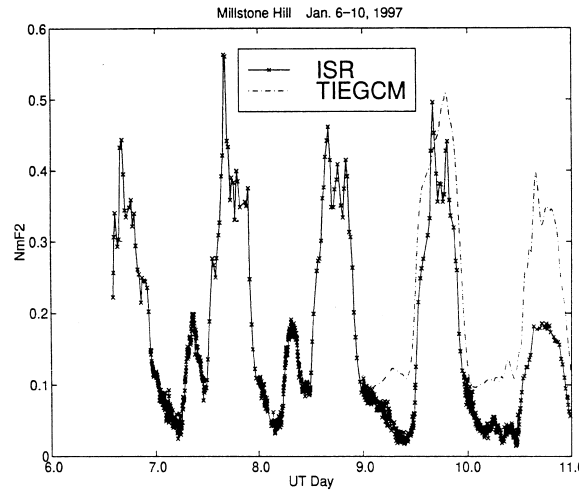

Fig. 8. Peak electron density (NmF2), in units of 10^{12} m^{-3}, as measured by the Millstone Hill (43°N, 289°E geographic, 53°N magnetic) incoherent-scatter radar for the five-day interval 1997 January 6–10. Corresponding simulations from the NCAR TIE-GCM are shown for the final two days. (From Buonsanto et al., 1999. Copyright by the American Geophysical Union.)

4. Traveling atmospheric disturbances

Superimposed on the global-scale changes discussed above are large structured transient disturbances. The rapidly varying magnetospheric energy inputs produce a large amount of spatial and temporal structure in the thermosphere during a storm. Impulses in the energy input launch waves that can propagate globally. Fig. 10 shows a simulation of a large-scale wave launched by a substorm, using a two-dimensional model (Richmond and Matsushita, 1975). The magnetic latitude of 30° is approximately that of Arecibo, while 50° is at upper midlatitudes, not too far from the latitude of Millstone Hill. At the upper altitudes the disturbance propagates equatorward at about 750 m/s, nearly the speed of sound in the upper thermosphere. The

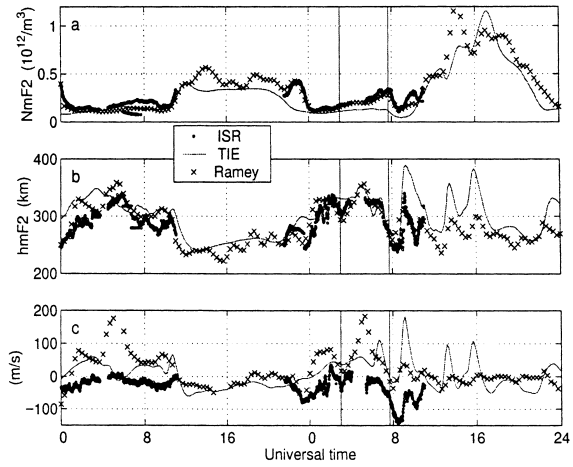

Fig. 9. Measurements and model values for 1997 January 9–10 from the Arecibo incoherent-scatter radar (ISR, circles), from the Ramey ionosonde (crosses), and from the NCAR TIE-GCM model simulation (TIE, continuous line). (a) Peak electron density. (b) Height of the electron density peak. (c) Vertical ion velocity (average of data from 250 to 400 km altitude) observed by the Arecibo radar, compared with winds in the magnetic meridian (positive southward) from the TIE-GCM at 300 km and from the servo model at hmF_2 at Ramey. The vertical solid lines indicate times of possible electric field penetration events. (From Buonsanto et al., 1999. Copyright by the American Geophysical Union.)

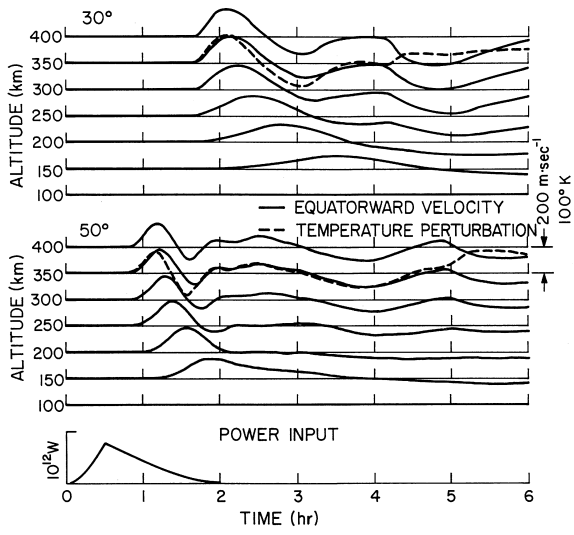

Fig. 10. Gravity-wave disturbances in the equatorward wind and in the temperature at 30° and 50° latitude from a two-dimensional simulation. The hemispherically integrated power input from auroral currents and particles in the auroral region, centered around 70° latitude, is shown at the bottom. (From Richmond and Matsushita, 1975. Copyright by the American Geophysical Union.)

disturbance can be described in terms of atmospheric gravity waves generated in the auroral zone primarily in the lower thermosphere, around 125 km, and propagating outward and upward into the upper thermosphere. The impulsive heat input generates a spectrum of waves that disperse as they propagate away from the source. Gravity waves propagate with a group velocity that usually has a much larger horizontal than vertical component. Lower-frequency gravity waves are constrained to travel at shallower inclinations from the horizontal than are higher-frequency waves, and the lower-frequency waves reach the upper thermosphere only at great distances from the source. Nearer the source they are seen only at the lower altitudes. Higher-frequency waves can propagate at larger inclination angles, and because they grow in amplitude with altitude as atmospheric density decreases, they dominate the prompt response at high altitudes for locations nearer the source. Above a given site, the gravity-wave disturbance appears to move downward, but this does not represent the group velocities of the constituent waves, which are arriving nearly horizontally from the distant source. At each altitude, the subsequent wave train, after the initial impulse, is fairly rapidly damped by viscosity and ion drag. The propagation speed of the disturbance is considerably faster than the wind speed itself. Notice that the wind and temperature perturbations are approximately in phase until the arrival of a disturbance originating in the opposite hemisphere (at time 4.2 h for 30° and 4.9 h for 50°), when the temperature perturbation becomes out of phase with the wind. Waves like this produce ionospheric disturbances that tend to propagate with the phase speed of the neutral disturbance.

The ionosphere over Arecibo showed irregular variation throughout the 1997 January 10 storm, but one particular feature was identified by Buonsanto et al. (1999) as being driven by a large traveling atmospheric disturbance, as seen in Fig. 9c. Shortly before 9 UT the ionosphere began to rise rapidly, and both the TIE-GCM and a so-called "servo" model of the wind estimated from the height of the ionosphere show a large equatorward pulse of wind.

5. Electric field penetration to low latitudes

The electric field imposed on the ionosphere at high latitudes almost instantaneously spreads out globally. The field that penetrates to middle and low latitudes is theoretically predicted to be damped on time scales of 30 min or so, due to an electrodynamic reaction of the magnetospheric plasma known as "shielding" (e.g. Southwood, 1977), although observational verification of the efficiency and rapidity of shielding has been difficult (e.g. Forbes et al., 1995). At middle and low latitudes the penetrating electric field can rapidly raise or lower the ionosphere, and help create or suppress plasma instabilities that create small-scale irregularities deleterious to transionospheric radio signals

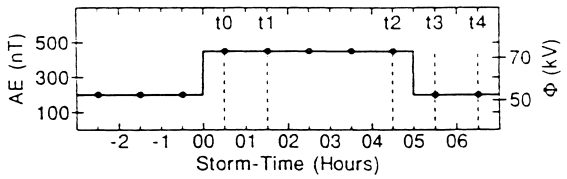

Fig. 11. Idealized time variations of the *AE* index and polar cap potential drop Φ characterizing the manner in which Jicamarca vertical ion drift data were binned in the study of Fejer and Scherliess (1995). Times $t0 - t4$ are characteristic storm phases for which the drifts are shown in Fig. 12. (From Fejer and Scherliess, 1995. Copyright by the American Geophysical Union.)

(e.g. Tanaka, 1981; Takahashi et al., 1987; Foster and Rich, 1998). At the magnetic equator, east-west electric fields only a few percent as strong as the high-latitude field can have a major impact on the ionosphere through the vertical drifts they create.

The strength and direction of the electric field that penetrates to the equator is highly variable, but in an innovative study Fejer and Scherliess (1995, 1997) have been able to extract the average behavior of the vertical drift as a function of local time from observations at the Jicamarca radar. By binning the data with respect to times of large increase or decrease in the auroral electrojet index *AE*, they were able to distinguish between quasi-steady-state variations and those that are inherently time-dependent. Fig. 11 shows an idealized storm representative of the way the data were binned, that is, before and after rapid increases or decreases in *AE*. Fig. 12 shows the average disturbance vertical drifts for the five times shown in Fig. 11, together with standard deviations from the binning. Shortly after an *AE* increase (time $t0$) the drift becomes more negative in the early morning and somewhat positive in the later part of the day. This perturbation tends to decay during the next hour ($t1$), apparently because of the shielding effect that then has time to become established.

Direct penetration of electric fields from the polar region is not the only source of disturbance equatorial electric fields. The altered thermospheric wind system also has an indirect influence, because it changes the ionospheric dynamo and its associated generation of electric fields. That is, Joule heating from the high-latitude winds changes the global thermospheric winds system, and this changed system changes the dynamo generation of electric fields. Simulation models (Blanc and Richmond, 1980; Richmond and Roble, 1997) have indicated that the "disturbance dynamo" electric field at the equator tends to be westward at day and eastward at night, basically a reduction in the quiet-day electric field, and generally opposite to the direction of the average direct-penetration electric field. This is consistent with the disturbance drifts at time $t2$ in Fig. 12, several hours after the start of the activity. When the storm turns off ($t3$), there is an additional transient drift that is like the negative of the

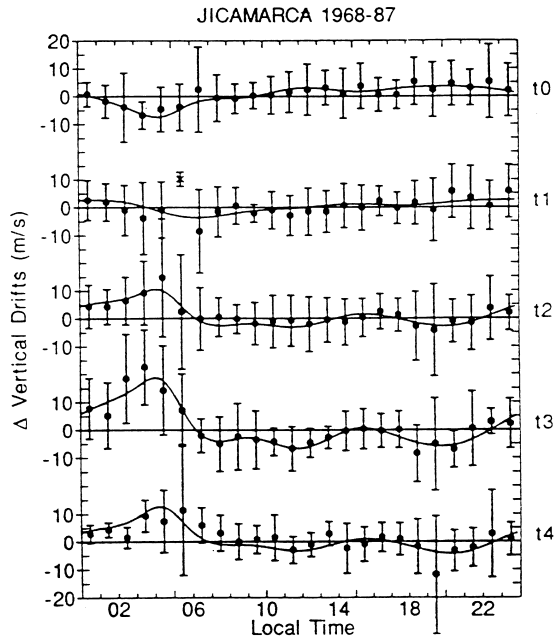

Fig. 12. Equatorial vertical drift perturbations for the conditions and at the five storm times $t0 - t4$ indicated in Fig. 11. The dots indicate the average perturbations velocities obtained by binning the data; the *X* denotes an average from less than 5 samples, and the vertical bars are the standard deviations. The solid curves indicate the velocity patterns determined from an analytical model. (From Fejer and Scherliess, 1995. Copyright by the American Geophysical Union.)

$t0$ drift, added to the $t2$ drift. When that transient decays, the disturbance dynamo drift remains ($t4$), because of the persistence of the disturbance winds that take many hours to relax back to the quiet state.

The ionosphere at low latitudes is very sensitive to electric fields. Fig. 13 compares simulations of electron densities along the 70°W geographic meridian at 21 UT (16.33 local time) for a reference quiet day (left) and for the disturbed day 1997 January 10 (right). During the day the normally eastward electric field causes the ionosphere to be lifted to high altitudes, where diffusion is very rapid along magnetic field lines. Gravity pulls the ions downward and poleward on either side of the magnetic equator, so that a trough develops over the equator, with density maxima to the north and south. (Note that the magnetic equator is at about 12°S geographic at this longitude.) This structure is referred to as the equatorial or Appleton anomaly. If the daytime eastward electric field is strengthened, the density maxima move further poleward and the ionospheric density over the equator is reduced. Conversely, if the eastward electric field is weakened, the maxima shift back toward the equator, and the equatorial density increases. One important effect of the latitudinal shift of the anomaly peaks is that the electron density over a site located at the edge of the anomaly is very

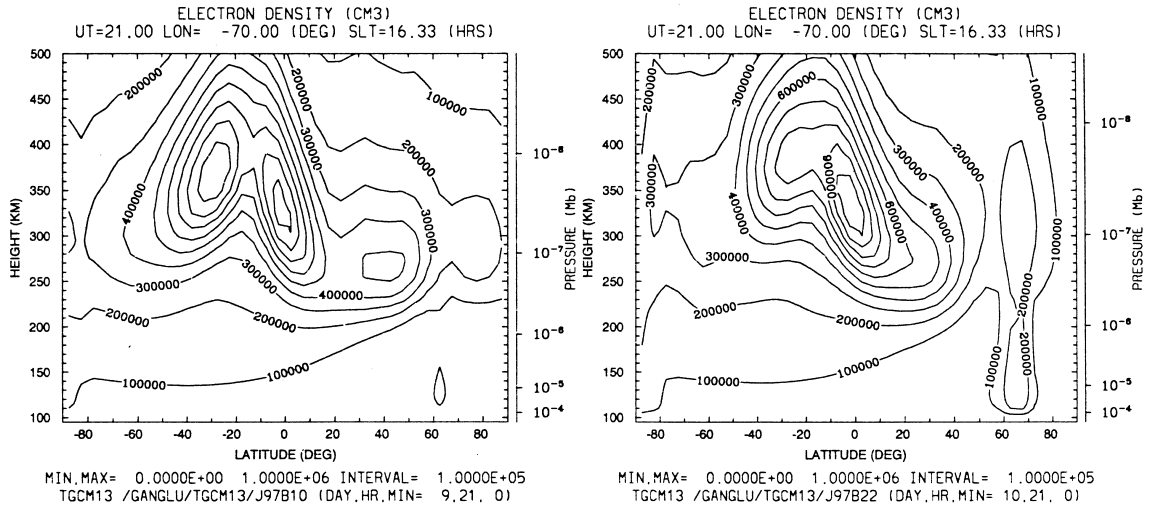

Fig. 13. Distributions of electron density simulated with the NCAR TIE-GCM along the −70° geographic meridian as a function of latitude and height at 21 UT (16:20 local time) on a quiet reference day (left) and on the storm day 1997 January 10 (right). Densities are in units of cm^{-3}.

sensitive to electric field changes. In this case the northern edge of the anomaly lay just south of Arecibo (18°N) on the quiet day, but expanded poleward over Arecibo on January 10. The asymmetry about the magnetic equator on January 10 is due in part to asymmetric meridional disturbance winds that tend to push the plasma up in the south but down in the north.

6. Importance of accurate magnetospheric inputs for modeling thermospheric/ionospheric storms

The complexity of upper atmospheric storms makes it very difficult to model or to forecast their detailed behavior accurately. Simulation models have been able to reproduce semiquantitatively the electron density increases and decreases observed during storms, including structures observed in polar regions and at low latitudes, and traveling disturbances seen at middle latitudes. However, reproducing the observed timing and locations of the increases and decreases is difficult. The polar ionospheric structure depends very much on the distributions of auroral particle precipitation and ion convection by electric fields. The boundary between midlatitude increases and decreases in ionospheric plasma density depends very much on the strength and distribution of Joule heating. Equatorial ionospheric changes depend very much on the amount of electric field penetration from polar regions, as well as on disturbance dynamo effects. One of the keys to improving the ability of simulation models to predict more accurately thermospheric and ionospheric storm behavior will be to get more accurate determinations of the the magnetospheric energy inputs at high latitudes through auroral precipitation and electric fields and currents.

Acknowledgements

We thank Chris Meyer for helpful comments. The National Center for Atmospheric Research is sponsored by the National Science Foundation (NSF). Additional support came from the National Space Weather Research Program and from the NASA Space Physics Theory Program.

References

Aarons, J., Lin, B., 1999. Development of high latitude phase fluctuations during the January 10, April 10,11, and May 15, 1997 magnetic storms. Journal of Atmospheric and Solar-Terrest Physics 61, 309–327.

Abdu, M.A., 1997. Major phenomena of the equatorial ionosphere–thermosphere system under disturbed conditions. Journal of Atmospheric and Solar-Terrest Physics 59, 1505–1519.

Bilitza, D. (Ed.), 1990. International Reference Ionosphere 1990. NSSDC 90-22, Greenbelt, MD.

Blanc, M., Richmond, A.D., 1980. The ionospheric disturbance dynamo. Journal of Geophysical Research 85, 1669–1686.

Brinkman, D.G., Walterscheid, R.L., Richmond, A.D., Venkateswaran, S.V., 1992. Wave-mean flow interaction in the storm-time thermosphere: a two-dimensional model simulation. Journal of the Atmospheric Sciences 49, 660–680.

Buonsanto, M.J., 1999. Ionospheric storms — a review. Space Science Reviews 88, 563–601.

Buonsanto, M.J., González, S.A., Lu, G., Reinisch, B.W., Thayer, J.P., 1999. Coordinated incoherent scatter radar study

of the January 1997 storm. Journal of Geophysical Research 104, 24,625–24,637.

Burns, A.G., Killeen, T.L., Crowley, G., Emery, B.A., Roble, R.G., 1989. On the mechanisms responsible for high-latitude thermospheric composition variations during the recovery phase of a geomagnetic storm. Journal of Geophysical Research 94, 16,961–16,968.

Elsen, R.K., Winglee, R.M., Spann, J.F., Germany, G.A., Brittnacher, M., Parks, G.K., 1998. The auroral oval boundaries on January 10, 1997: a comparison of global magnetospheric simulations with UVI images. Geophysical Research Letters 25, 2585–2588.

Fejer, B.G., Scherliess, L., 1995. Time dependent response of equatorial ionospheric electric fields to magnetospheric disturbances. Geophysical Research Letters 22, 851–854.

Fejer, B.G., Scherliess, L., 1997. Empirical models of storm time equatorial zonal electric fields. Journal of Geophysical Research 102, 24,047–24,056.

Field, P.R., Rishbeth, H., Moffett, R.J., Idenden, D.W., Fuller-Rowell, T.J., Millward, G.H., Aylward, A.D., 1998. Modelling composition changes in F-layer storms. Journal of Atmospheric Solar-Terrest Physics 60, 523–543.

Forbes, J.M., Roble, R.G., Marcos, F.A., 1995. Equatorial penetration of magnetic disturbance effects in the thermosphere and ionosphere. Journal of Atmospheric Terrest Physics 57, 1085–1093.

Foster, J.C., Rich, F.J., 1998. Prompt midlatitude electric field effects during severe geomagnetic storms. Journal of Geophysical Research 103, 26,367–26,372.

Fuller-Rowell, T.J., Codrescu, M.V., Moffett, R.J., 1994. Response of the thermosphere and ionosphere to geomagnetic storms. Journal of Geophysical Research 99, 3893–3914.

Fuller-Rowell, T.J., Codrescu, M.V., Quegan, S., 1996. On the seasonal response of the thermosphere and ionosphere to geomagnetic storms. Journal of Geophysical Research 101, 2343–2353.

Fuller-Rowell, T.J., Codrescu, M.V., Roble, R.G., Richmond, A.D., 1997. How does the thermosphere and ionosphere react to a geomagnetic storm? In: Magnetic Storms, AGU Geophysical Monograph, Vol. 98, pp. 203–225.

Greenwald, R.A., Baker, K.B., Dudeney, J.R., Pinnock, M., Jones, T.B., Thomas, E.C., Villain, J.-P., Cerisier, J.-C., Senior, C., Hanuise, C., Hunsucker, R.D., Sofko, G., Koehler, J., Nielsen, E., Pellinen, R., Walker, A.D.M., Sato, N., Yamagishi, H., 1995. DARN/SuperDARN, a global view of the dynamics of high-latitude convection. Space Science Reviews 71, 761–796.

Hairston, M.R., Weimer, D.R., Heelis, R.A., Rich, F., 1999. Analysis of the ionospheric cross polar cap potential drop and electrostatic potential distribution patterns during the January 1997 CME event using DMSP data. Journal of Atmospheric Solar-Terrest Physics 61, 195–206.

Hedin, A.E., 1991. Extension of the MSIS thermosphere model into the middle and lower atmosphere. Journal of Geophysical Research 96, 1159–1172.

Ho, C.M., Mannucci, A.J., Lindqwister, U.J., Pi, X., Tsurutani, B.T., Sparks, L., Iijima, B.A., Wilson, B.D., Harris, I., Reyes, M.J., 1998. Global ionospheric TEC variations during January 10, 1997 storm. Geophysical Research Letters 25, 2589–2592.

Jakowski, N., Schlüter, S., Sardón, E., 1999. Total electron content of the ionosphere during the geomagnetic storm on 10 January 1997. Journal of Atmospheric Solar-Terrest Physics 61, 299–307.

Lu, G., Baker, D.N., Farrugia, C.J., Lummerzheim, D., Ruohoniemi, J.M., Rich, F.J., Evans, D.S., Lepping, R.P., Brittnacher, M., Li, X., Greenwald, R., Sofko, G., Villain, J., Lester, M., Thayer, J., Moretto, T., Milling, D., Troshichev, O., Zaitzev, A., Makarov, G., Hayashi, K., 1998. Global energy deposition during the January 1997 magnetic cloud event. Journal of Geophysical Research 103, 11,685–11,694.

Maeda, S., Fuller-Rowell, T.J., Evans, D.S., 1989. Zonally averaged dynamical and compositional response of the thermosphere to auroral activity during September 18–24, 1984. Journal of Geophysical Research 94, 16,869–16,883.

McEwen, D.J., Steele, D.P., Creutzberg, F., Wallis, D.D., 1999. The ionospheric response to the CME event of 6–11 January 1997. Journal of Atmospheric Solar-Terrest Physics 61, 223–232.

Mikhailov, A.V., Förster, M., 1999. Some F_2-layer effects during the January 06–11, 1997 CEDAR storm period as observed with the Millstone Hill incoherent scatter facility. Journal of Atmospheric Solar-Terrest Physics 61, 249–261.

Prölss, G.W., 1981. Latitudinal structure and extension of the polar atmospheric disturbance. Journal of Geophysical Research 86, 2385–2396.

Prölss, G.W., 1993. On explaining the local time variation of ionospheric storm effects. Annales de Geophysicae 11, 1–9.

Prölss, G.W., 1995. Ionospheric F-region storms. In: Volland, H. (Ed.), Handbook of Atmospheric Electrodynamics, Vol. II. CRC Press, Boca Raton, FL, pp. 195–248.

Prölss, G.W., 1997. Magnetic storm associated perturbations of the upper atmosphere. In: Magnetic Storms, AGU Geophysical Monograph, Vol. 98.

Prölss, G.W., von Zahn, U., 1977. Seasonal variations in the latitudinal structure of atmospheric disturbances. Journal of Geophysical Research 82, 5629–5632.

Rees, D., 1995. Observations and modelling of ionospheric and thermospheric disturbances during major geomagnetic storms: a review. Journal of Atmospheric Solar-Terrest Physics 57, 1433–1457.

Rees, D., Smith, R.W., Signernes, F., Henriksen, K., Brandstrom, U., Harris, M., Maskall, G., 1998. Observations of thermospheric neutral winds within the polar cusp and the auroral oval using a Doppler imaging system (DIS). Annales de Geophysicae 16, 1461–1474.

Rees, M.H., Emery, B.A., Roble, R.G., Stamnes, K., 1983. Neutral and ion gas heating by auroral electron precipitation. Journal of Geophysical Research 88, 6289–6300.

Richmond, A.D., Matsushita, S., 1975. Thermospheric response to a magnetic substorm. Journal of Geophysical Research 80, 2839–2850.

Richmond, A.D., Roble, R.G., 1997. Electrodynamic coupling effects in the thermosphere/ionosphere system. Advances in Space Research 20, 1115–1124.

Rishbeth, H., 1991. F-region storms and thermospheric dynamics. Journal of Geomagnetism and Geoelectricity 43 (Suppl.), 513–524.

Rodger, A.S., Wrenn, G.L., Rishbeth, H., 1989. Geomagnetic storms in the Antarctic F-region. II. Physical interpretation. Journal of Atmospheric Solar-Terrest Physics 51, 851–866.

Sánchez, E.R., Thayer, J.P., Kelly, J.D., Doe, R.A., 1998. Energy transfer between the ionosphere and magnetosphere during the January 1997 CME event. Geophysical Research Letters 25, 2597–2600.

Schlegel, K., Collis, P.N., 1999. The storm of January 10, 1997: electrodynamics of the high latitude E region from EISCAT data. Journal of Atmospheric Solar-Terrest Physics 61, 217–222.

Schunk, R.W., Sojka, J.J., 1996. Ionosphere–thermosphere space weather issues. Journal of Atmospheric Solar-Terrest Physics 58, 1527–1574.

Schunk, R.W., Banks, P.M., Raitt, W.J., 1976. Effects of electric fields and other processes upon the nighttime high-latitude *F* layer. Journal of Geophysical Research 81, 3271–3282.

Sivjee, G.G., 1999. Polar thermospheric response to solar magnetic cloud/coronal mass ejection interactions with the magnetosphere. Journal of Atmospheric Solar-Terrest Physics 61, 207–215.

Smith, R., 1998. Vertical winds: a tutorial. Journal of Atmospheric Solar-Terrest Physics 60, 1425–1434.

Sojka, J.J., Schunk, R.W., Bowline, M.D., Chen, J., Slinker, S., Fedder, J., Sultan, P.J., 1998. Ionospheric storm simulations driven by magnetospheric MHD and by empirical models with data comparisons. Journal of Geophysical Research 103, 20, 669–20,684.

Southwood, D.J., 1977. The role of hot plasma in magnetospheric convection. Journal of Geophysical Research 82, 5512–5520.

Spann, J.F., Brittnacher, M., Elsen, R., Germany, G.A., Parks, G.K., 1998. Initial response and complex polar cap structures of the aurora in response to the January 10, 1997 magnetic cloud. Geophysical Research Letters 25, 2577–2580.

Steele, D.P., McEwen, D.J., 1998. Ground-based optical observations from the north magnetic pole during the January 1997 magnetic cloud event. Geophysical Research Letters 25, 2573–2576.

Takahashi, T., Oya, H., Watanabe, S., 1987. Ionospheric disturbances induced by substorm associated electric fields in the low-latitude *F*-region. Journal of Geomagnetism and Geoelectricity 39, 187–209.

Tanaka, T., 1981. Severe ionospheric disturbances caused by the sudden response of evening subequatorial ionospheres to geomagnetic storms. Journal of Geophysical Research 86, 11,335–11,349.

Wrenn, G.L., Rodger, A.S., Rishbeth, H., 1987. Geomagnetic storms in the Antarctic *F*-region. I. Diurnal and seasonal patterns for main phase effects. Journal of Atmospheric Solar-Terrest Physics 49, 901–913.